Materials Transactions, Vol. 45, No. 7 (2004) pp. 2316 to 2325

Stored Energy and Taylor Factor Relation in an Al-Mg-Mn Alloy Sheet Worked by Continuous Cyclic Bending

Yoshimasa Takayama[1,2] and Jerzy A. Szpunar[2]

[1]*Department of Mechanical Systems Engineering, Utsunomiya University, Utsunomiya 321-8585, Japan*
[2]*Department of Metallurgical Engineering, McGill University, Montreal, Quebec, H3A 2B2, Canada*

The relation between the stored energy and the Taylor factor (TF) has been investigated using the SEM/EBSP analysis in an Al-Mg-Mn alloy sheet worked by the continuous cyclic bending (CCB). The analysis reveals that the stored energy is high for the high TF region, whereas a significant increase of the stored energy with the decrease of the Taylor factor appears in the vicinity of the minimum TF value of 2. This observation is discussed using the Schmid factor calculated. Further, the local strain accommodation during deformation is analyzed for grains of different orientations. The stored energy is derived from the calculation based on the kernel average misorientation (KAM).

(Received March 29, 2004; Accepted May 24, 2004)

Keywords: *stored energy, Taylor factor, continuous cyclic bending, misorientation, electron back scatter diffraction pattern (EBSP) technique, Schmid factor, aluminium-magnesium-manganese alloy*

1. Introduction

Recrystallization textures developed during annealing are governed by the energy stored in deformation state. It is well known that the stored energy depends on crystallographic orientation.[1)] Alternatively, this is the reason why the recrystallization texture forms. Several attempts have been made to evaluate the stored energy by calorimetric[2,3)] and diffraction techniques.[4–9)] The latter technique is divided into two types. One is the basic method[4–6)] in which X-ray line broadening is measured to obtain the stored energy in grains having specific orientations, for example (100) plane parallel to the rolling plane in the sample. Another is the extended method[7–10)] which was used to determine the stored energy for a much wider space described by the orientation distribution function. Using the extended method, Kallend and Huang, Gerber *et al.*,[7,10)] Rajmohan *et al.*[8)] and Rajmohan and Szpunar[9)] carried out the measurement of the stored energy in copper, interstitial free steel and can body aluminum alloy after rolling. They also investigated the relation between the stored energy and the Taylor factor[11)] which shows the total slip system activity expected during the deformation of a grain of specific orientation. Although the stored energy increases with an increase in the Taylor factor, the obtained results indicated some exceptions and a lot of scatter. It was understood that these exceptions and the scatter were attributed to the rotation of the grain orientation to the final one and the inhomogeneity of the deformation.

In the present study, the stored energy was evaluated from electron backscatter diffraction patterns in scanning electron microscopy (SEM/EBSP).[12,13)] The main application of SEM/EBSP technique is the measurement of local orientation data. Recrystallized material tends to be free of dislocations whereas deformed material will contain dislocations. One type of evidence for existence of dislocations is misorientation between small elements of deformed material or subgrains. Thus, the stored energy can be approximated and analyzed by measuring the local misorientation.

The continuous cyclic bending (CCB), which is one of straining techniques proposed for microstructural control of rolled metals, can produce the high strain in the surface layer and the low strain in the central part of metal sheets.[14)] This straining technique with cyclic deformation leads to a definite difference in strain between the surface and central layers. It was reported that the CCB and subsequent annealing made it possible to produce the gradient microstructure with the coarse-grained surface and the fine-grained central layers in an Al-4.7%Mg-0.7%Mn alloy (A5083)[15)] and commercial purity titanium sheets.[16)] The formation of the coarse-grained layers in the Al-Mg-Mn alloy was related with sharpening of cube texture.[15)] Further, it should be noted that the CCB can give the materials very large strain, nevertheless imposes no apparent rotation of grains during straining.

The aim of the present paper is to clarify the relation between the stored energy and the Taylor factor for the prediction of recrystallization texture development using a favorable sample of a CCBent aluminum alloy sheet and an appropriate technique of the SEM/EMSP.

2. Experimental Procedure

The Al-4.7 mass%Mg-0.7 mass%Mn (A5083) alloy used in the present study was produced by the Sky Aluminum Company, Japan. The material was received in the form of rolled sheets of 1.5 mm thick, and the same one as used in the previous studies.[14,15)] The as-received sheets had been manufactured by the process of casting, homogenizing (at 803 K), hot rolling, cold rolling with a reduction of 75% and a final continuous annealing at 673 K. Workpiece was machined with a 500 mm length, a 20 mm width and a 1.5 mm thickness, and then was cyclic-bent continuously using a specially-designed device up to the number of passes, $N_{CCB} = 50$. The cumulative true strain is estimated as 5.28.[15)] The CCB passes were carried out on both sides of the sheet alternately to keep the symmetry of straining. The longitudinal direction is parallel to the rolling direction. The sample coordinate system is defined by the rolling, transverse and normal directions (RD, TD and ND) according to common practice for rolled sheets. From the CCBent workpiece and the as-received sheet the specimens with

dimension of 25 mm × 15 mm × 1.5 mm were prepared for the grain orientation analysis that was performed using the electron backscatter diffraction pattern (EBSP) technique by TSL Orientation Image Microscopy (OIM) system and Philips FE-SEM.

3. Taylor Factor in Continuous Cyclic Bending

3.1 Deformation gradient tensor in the CCB

In order to determine the Taylor factor, the deformation gradient tensor F is required. It is well known that tension is induced in the outer side of a sheet for bending while compression in the inner side. Neutral curved interface, which exists in the short transverse direction of the bent sheet, does not always lie in the center. Consider strains, ε_b, ε_t and ε_θ, in the width, thickness and tangential directions for the outer side of the bent sheet. When the width is fairly larger than the thickness of the sheet, the plane strain state with $\varepsilon_b = 0$ is in the center.[17] The ratio $-\varepsilon_b/\varepsilon_\theta$ depends upon the sheet width and curvature. Radius of curvature in the CCB, which is about 14 times larger than thickness of sheet, is large enough to neglect its effect. According to the previous experimental result,[17] $-\varepsilon_b/\varepsilon_\theta$ is zero in the region far from the edge by distance of more than three times of sheet thickness. Therefore, the deformation gradient tensor in the center region of the CCBent sheet having large width/thickness ratio is equivalent to that in rolling as follows:

$$\boldsymbol{F} = \begin{bmatrix} 1 & 0 & 0 \\ 0 & 0 & 0 \\ 0 & 0 & -1 \end{bmatrix} \tag{1}$$

3.2 Taylor factor distribution in a 50-pass CCBent sample

We analyzed grain orientation distribution data obtained by the SEM/EBSP technique in the surface of 50-pass CCBent sample. Figure 1 illustrates a Taylor factor (TF) map in the CCBent sample. We classified Taylor factors into low [2.0, 2.8], middle (2.8, 3.4] and high (3.4, 5.0) TF ranges. This classification made the three classes of grains occupying almost the same area of the sample. The mean TF is calculated to be 3.206 using the OIM software. No spatial concentration of grains belonging to each TF class is observed in the figure.

4. Intragranular Misorientation in CCBent Sample

Intragranular misorientation in SEM/EBSP data reflects stored energy because it results from presence and arrangement of dislocations. Variation of the intragranular dislocation density was already interpreted as a function of intragranular misorientation.[18] It was found that a high dislocation density was always associated with a high misorientation, but the reverse was not true. Using the 50pass-CCBent sample data, intragranular misorientations were investigated both along RD and TD for ten grains of each TF region. Typical profiles of intragranular misorientations for grains with low and high Taylor factors are displayed in Fig. 2. The distance in the figure is taken as long as possible for a grain along each direction, and is almost corresponding to each grain size. Point to point (P-to-P) and point to origin (P-to-O) imply nearest-neighbor and cumulative misorientation data, respectively. The P-to-O data both in RD and TD demonstrate differences between low and high TF grains. The misorientation increases rather smoothly with the distance in the low TF while it changes with characteristic fluctuations in the high TF curve. Such fluctuation seems to be especially remarkable in TD. This suggests complicated actions of plural glide systems in the high TF region. The drastic and recurring variations of the P-to-P misorientations also support this observation in the high TF, especially along TD. Figure 3 shows peak misorientations within different grains as a function of the measured distance. Generally speaking, the largest peak misorientation appears in the largest grains for both directions. The relatively large spread is observed in RD, and for low TF of point to point. The large spread of the misorientation for the low TF is consistent with high spread of stored energy reported in the IF steels.[8]

The results of the misorientations measured in the 50P sample are summarized in Table 1. All of misorientations and distances here represent mean values for the ten grains. The difference in the step-size of SEM/EBSP analysis between in RD and TD is due to the use of triangle lattice of measuring points. There is also difference in the distance between both the directions. The difference is attributed not only to the whole strain generated by the CCB, about 3% in RD[14] but also to the original microstructure of the rolled sheet. The distance will be used for normalization of the misorientation data below.

Interesting facts are found for the peak misorientations. The peak of the P-to-P in RD for the high TF (HTF) grains is the largest, which implies the largest strain. The peak for the low TF (LTF) grains is somewhat *larger* than that for the middle TF (MTF) grains, contrary to the expectation of the Taylor model with an underlying assumption that an applied stress in a grain is independent of a plastic strain. In TD, the peak for the LTF is the largest. The P-to-O misorientation is normalized by the analyzed distance to remove the dependence on the distance. The normalized P-to-O misorientations tend to decrease as the Taylor factor increases. This suggests that for the LTF grains, restricted slip systems act compared with for the higher TF, and then the larger P-to-O forms in the wider slip band owing to the larger slip distance per an active slip system. The mean P-to-P data also seem to show the similar tendency partly as well as the peak. The tendency reflects number of active slip systems for the distance of the step size. On the other hand, the difference in the standard deviation for the P-to-P is almost corresponding to that in the mean value and represents little change in inhomogeneity of misorientation because the variation coefficient, which is the standard deviation divided by the mean value, is roughly equivalent for all TF regions.

5. Relation between Taylor Factor and Kernel Average Misorientation

5.1 Kernel average misorientation

In the previous chapter, it is found that the intragranular

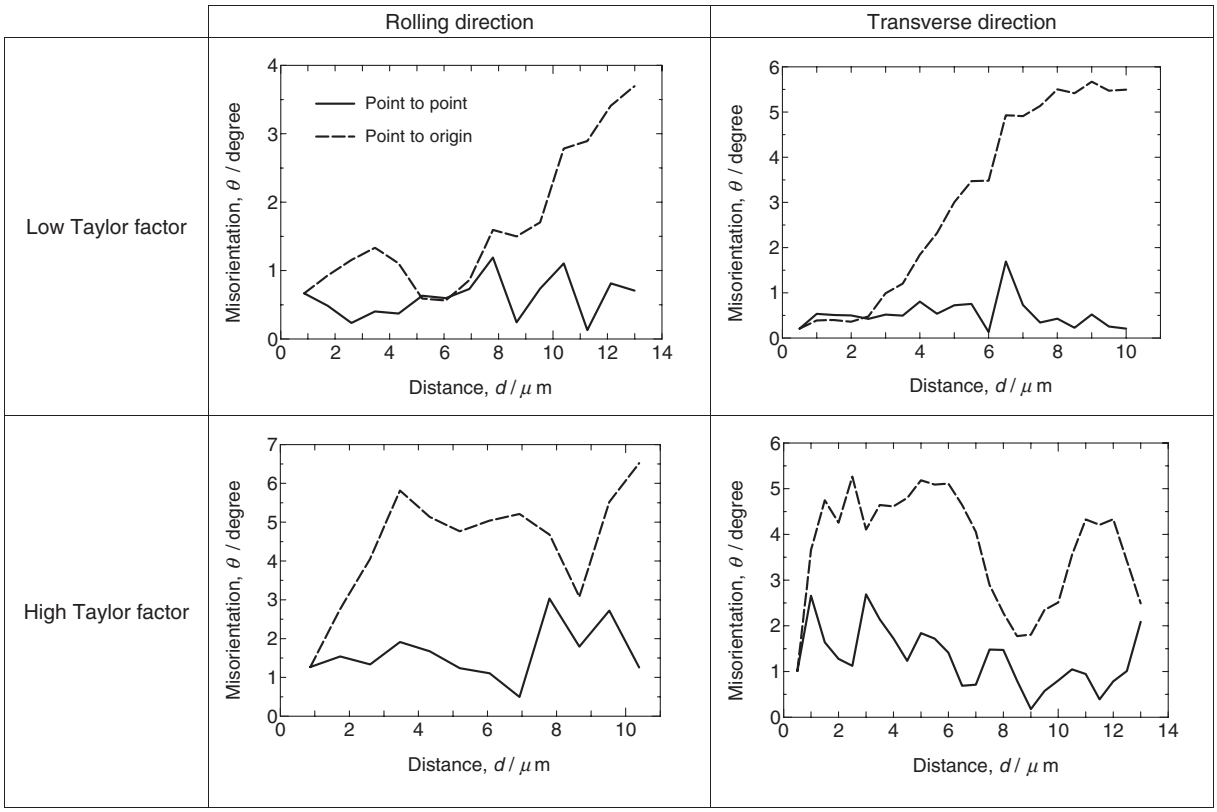

Fig. 2 Intragranular misorientation profiles in rolling and transverse directions for grains with low and high Taylor factors.

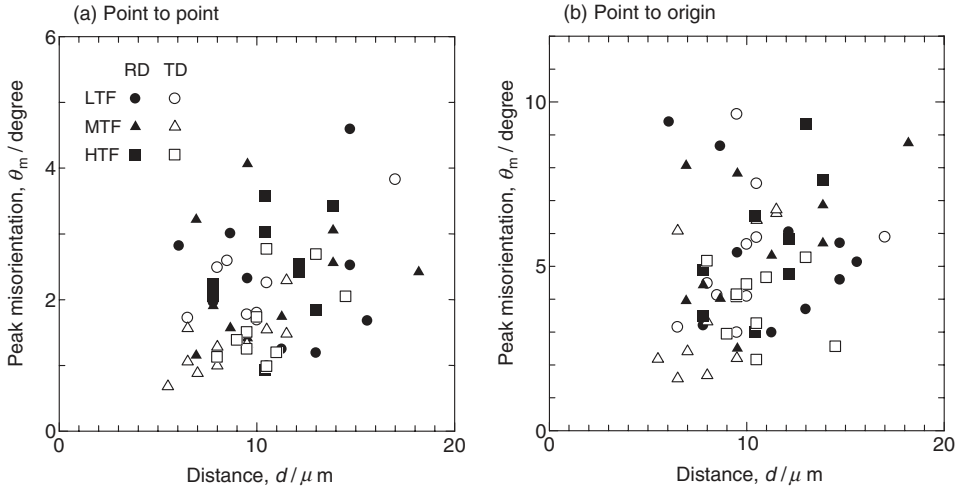

Fig. 3 Peak misorientations within different grains as a function of measured distance: (a) point-to-point and (b) point-to-origin.

misorientation is strongly related to the Taylor factor. The misorientation reflects the stored strain energy. The most appropriate quantity is "kernel average misorientation (KAM)" to evaluate the stored energy for a given point. The KAM is defined for a given point as the average misorientation of that point with all of its neighbors,[13] which is calculated with the proviso that misorientations exceeding a tolerance value of 5° are excluded from averaging calculation. The magnitude of the KAM is affected by the scan step size, which was always set as 0.5 μm in the present paper.

Figure 4 displays a KAM map of the 50-pass CCBent sample. The figure shows that high KAM areas are partially concentrated in groups of several grains, although the groups are distributed in the whole analyzed area. The high KAM areas sometimes connect with each other. The concentration of high KAM to vicinities of grain boundary seems not to be so frequent. Comparing the KAM map to the Taylor factor map (Fig. 1), one can conclude that some concentrations along the grain boundaries are observed in the LTF region rather than in the HTF one.

In order to investigate relation between the Taylor factor

Table 1 Intragranular misorientation analyses of each Taylor factor region for a 50-pass CCBent sample: LTF, MTF and HTF mean regions with Taylor factor ranged of 2.0-2.8, 2.8-3.4 and 3.4-5.0, respectively. P-to-P and P-to-O refer to misorientations for point-to-point and point-to-origin. SD and CV indicate standard deviation and variation coefficient, respectively.

		Analytical condition		Peak misorientation/degree				Mean, SD and VC for P-to-P/degree		
		Step-size /μm	Distance /μm	Number	P-to-P	P-to-O	P-to-O /Distance	Mean	SD	VC
LTF	RD	0.866	11.3	131	2.39	5.48	0.56	1.15	0.59	0.51
	TD	0.5	10.0	200	2.04	5.34	0.55	0.80	0.44	0.55
	Mean		10.7	166			0.55			
MTF	RD	0.866	10.7	123	2.31	5.74	0.57	1.01	0.59	0.59
	TD	0.5	8.5	169	1.31	3.92	0.45	0.63	0.32	0.52
	Mean		9.6	146			0.51			
HTF	RD	0.866	12.0	138	2.58	6.22	0.52	1.13	0.65	0.58
	TD	0.5	10.6	211	1.67	3.87	0.38	0.70	0.40	0.58
	Mean		11.3	175			0.45			

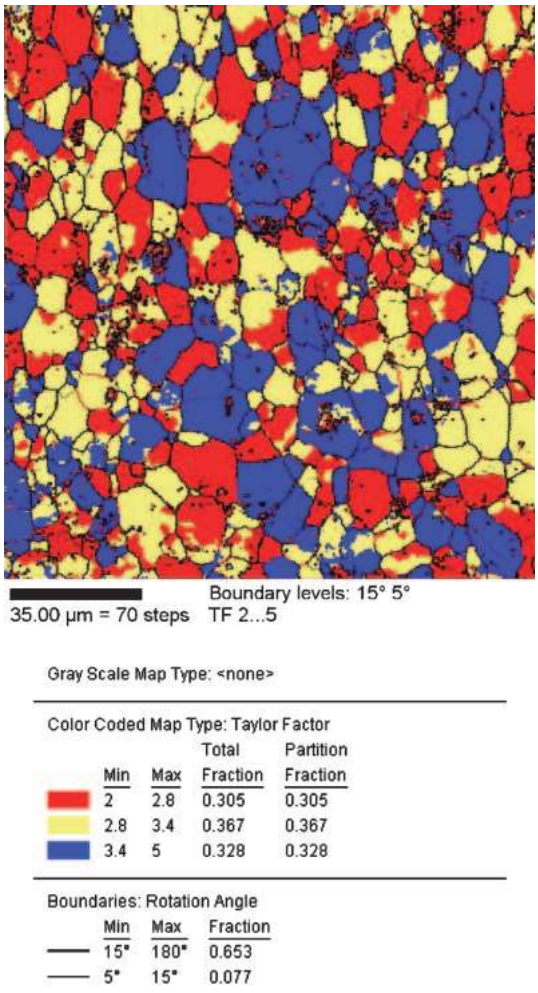

Fig. 1 Taylor factor map of the 50pass-CCBent sample.

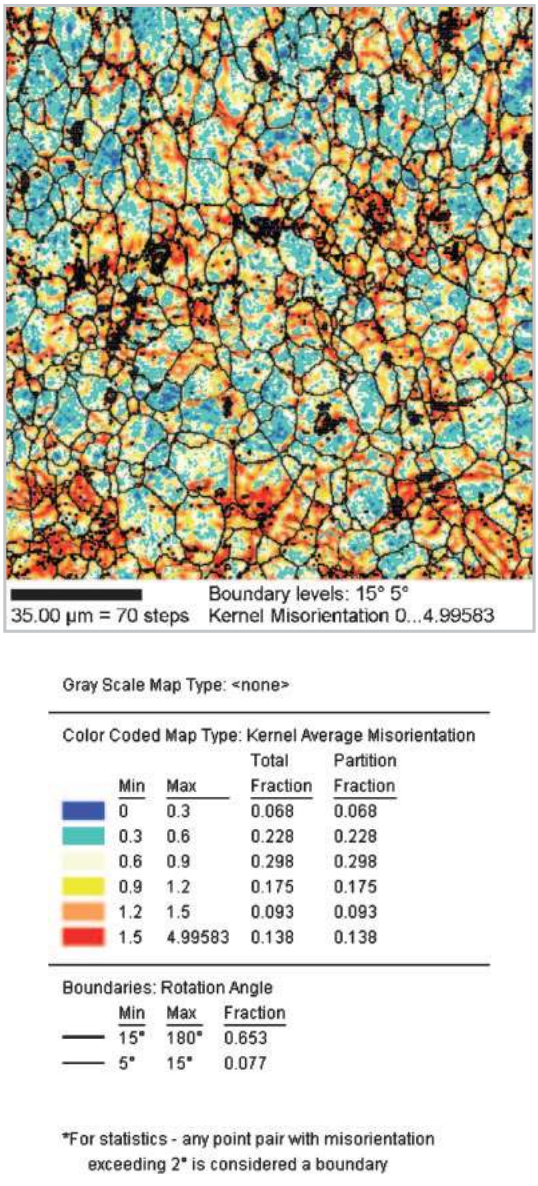

Fig. 4 Kernel average misorientation map of the 50-pass CCBent sample. The kernel average misorientation (KAM) is regarded as a criterion of stored energy.

and the KAM, the KAM distributions in the three Taylor factor regions are compared. Histograms of the KAM are shown for the whole field and the three regions in Fig. 5. The KAM distribution for the whole field has a peak at about 0.7 and a mean value of 0.980 [degree], which is regarded as a standard model in the CCBent sample. The number fraction

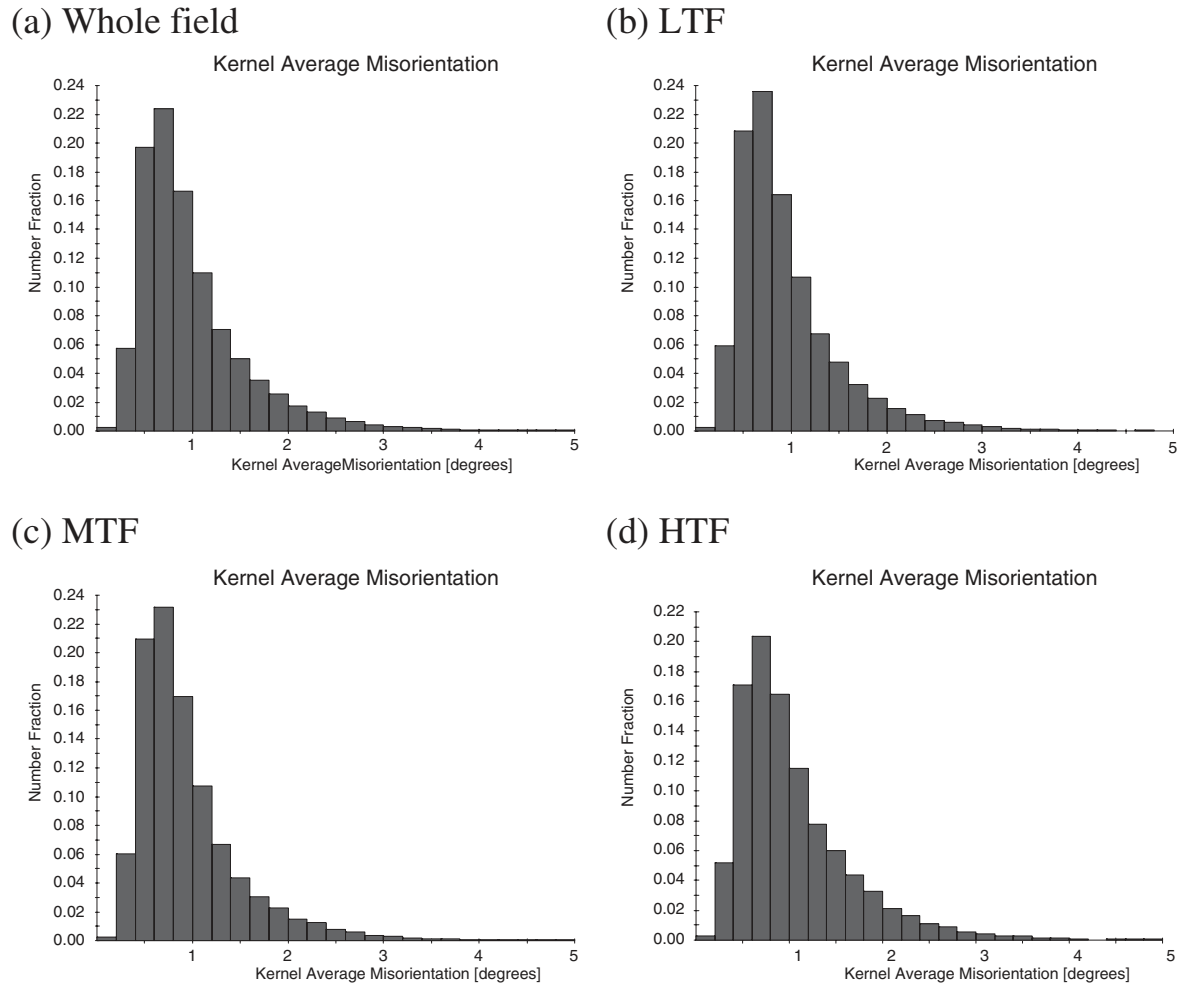

Fig. 5 Histograms of kernel average misorientation (KAM): (a) whole field [mean KAM: 0.980 degree], (b) low Taylor factor [0.946 degree], (c) middle Taylor factor [0.948 degree] and (d) high Taylor factor regions [1.048 degree].

of the KAM more than 1°, $f_{[\theta>1]}$ is 33.0%. The distribution for the LTF is relatively sharp, and of a smaller mean value of 0.946. Almost the same distribution is obtained for the MTF, which is not distinguished apparently from that for the LTF. The KAM for the HTF is distributed widely and typically. It is characterized by the lower peak and wider spread to the right side, and moreover, the fraction $f_{[\theta>1]}$ beyond 40%. In addition, a large mean value of 1.048 for the HTF indicates that the magnitude of the stored energy can be related to prediction of the Taylor model.[11)]

The more detailed analysis of the relation between the KAM and the Taylor factor requires calculation of the KAM for divided regions with a Taylor factor ranging at small intervals. Figure 6 shows (a) the mean KAM and (b) the fraction of points with a KAM more than 1°, as a function of the Taylor factor, respectively. The results for the as-received sample (0P) are also shown for comparison. Since the number fraction of the KAM not more than 1° was 96.6% for the 0P sample, the fraction is selected as another index of the stored energy. The index represents the fraction of the region definitely affected by deformation, namely the underestimated fraction. The mean value and the fraction for the misorientation higher than 1° exhibit a similar variation against the Taylor factor. The KAM fraction decreases noticeably with the Taylor factor, and then from Taylor factor about 2.8 increases slightly and finally from about 4.2 it rises considerably. It should be noted that the mean KAM increases even as the Taylor factor decreases in the low TF range. This reveals that the LTF grains practically deform with more strain than specified by the Taylor model.[11)] It is also found that a minimum strain is given by the CCB to the grains with a Taylor factor of about 2.8.

5.2 Effect of Schmid factor

The reason why the mean KAM increases with the decrease of the Taylor factor in the low TF range is discussed based on the Schmid factor. The LTF grains are not difficult to deform, and require only a small amount of the total slip on all active slip systems. Actually inhomogeneity of strain within the grain is caused by differences in deformability of grains of different orientation in a given stress state. This means the actual deformation needs local stress equilibrium between differently oriented grains, which is assumed by the Sachs model.[19)]

The Schmid factor for uniaxial tension in RD, which corresponds to a maximum principle stress in the stress state of the CCB, was distributed in the CCBent sample in the range from 0.273 to 0.5. The number fraction of the Schmid

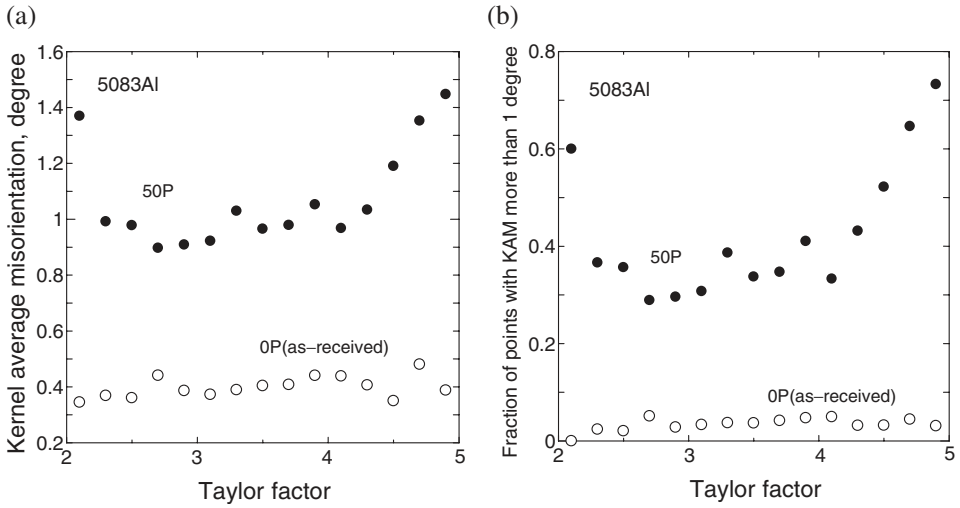

Fig. 6 Relation between kernel average misorientation (KAM) and Taylor factor: (a) mean KAM and (b) fraction of points with a KAM more than 1°.

Table 2 Mean KAM values in various TF regions and SF ranges.

Unit: degree

Schmid factor	Whole field	Taylor factor		
		LTF	MTF	HTF
LSF (0.27–0.38)	0.935	—	—	0.935
MSF (0.38–0.44)	0.994	0.927	0.956	1.083
HSF (0.44–0.47)	1.015	1.025	0.930	1.224
VHSF (0.47–0.5)	0.955	0.903	0.963	1.117

factor more than 0.44 exceeds 60%. Then, the Schmid factors (SF) were classified into four ranges of LSF [0.27, 0.38], MSF (0.38, 0.44], HSF (0.44, 0.47] and VHSF, which is the abbreviation for very high Schmid factor, (0.47, 0.50]. The mean KAM are listed with Taylor and Schmid factors in Table 2. In the whole field analyzed in the CCBent sample, the KAM values are calculated as 0.935 [degree] for the LSF, 0.994 for the MSF, 1.015 for the HSF and 0.955 for the VHSF. There is a trend that the mean KAM increases with the increase of the Schmid factor, except that the KAM in the VHSF is smaller even than that in the MSF. The exception is likely related to dependence of mobile dislocation density on grain orientation or the Schmid factor in the CCB. The dislocations caused in the very high SF (VHSF) grains include many mobile ones because they are generated by a smaller shear stress, and moreover, accompanied with less lattice distortion owing to the smaller shear stress and small stress component normal to slip plane. Since some of the mobile dislocations generated in tension can disappear in compression under the *cyclic* deformation of the CCB, they make no contribution to storage of strain energy. Then, the SF is analyzed in each TF range. The SF distribution in the LTF region is narrowly distributed from 0.409 to 0.5. The mean KAM was calculated as 0.927 [degree] for the MSF, 1.025 for the HSF and 0.903 for the VHSF. We also confirm that the very small KAM is obtained in the LTF-VHSF while the KAM in the LTF-HSF is considerably large. The former result supports the above idea about relation between the Schmid factor and the mobile dislocations. The latter one reveals that large strain is imposed on the LTF grain when it possesses enough high SF. The deformation proceeds easily in the grains oriented with the high TF and high SF as represented in the table. It is, therefore, clear that the SF effect is not negligible for the analysis of the stored strain energy in deformed materials.

6. Local Strain Analysis Based on Kernel Average Misorientation

It was found that the strain due to the CCB was not a simple increasing function of the Taylor factor as mentioned above. The detailed analysis revealed that the imposed strain depended on the Taylor and the Schmid factors, and suggested the significance of the local stress equilibrium accommodated by local deformation in the vicinity of grain boundaries. There is a special interest in the deformation of Cube component which is the main component of recrystallization texture in the present sample. Local strain analyses are performed here for high KAM grains and Cube grains, and their neighbors.

6.1 High KAM grains

Figure 7 illustrates (a) kernel average misorientation and (b) Taylor factor maps in a certain low TF grain and its neighbors. The grain has the near-Goss orientation $\{011\}\langle 100\rangle$. As shown in Fig. 7(a), the grain in the center stores a large amount of strain energy, while neighboring grains store only a small amount. The average Taylor factor

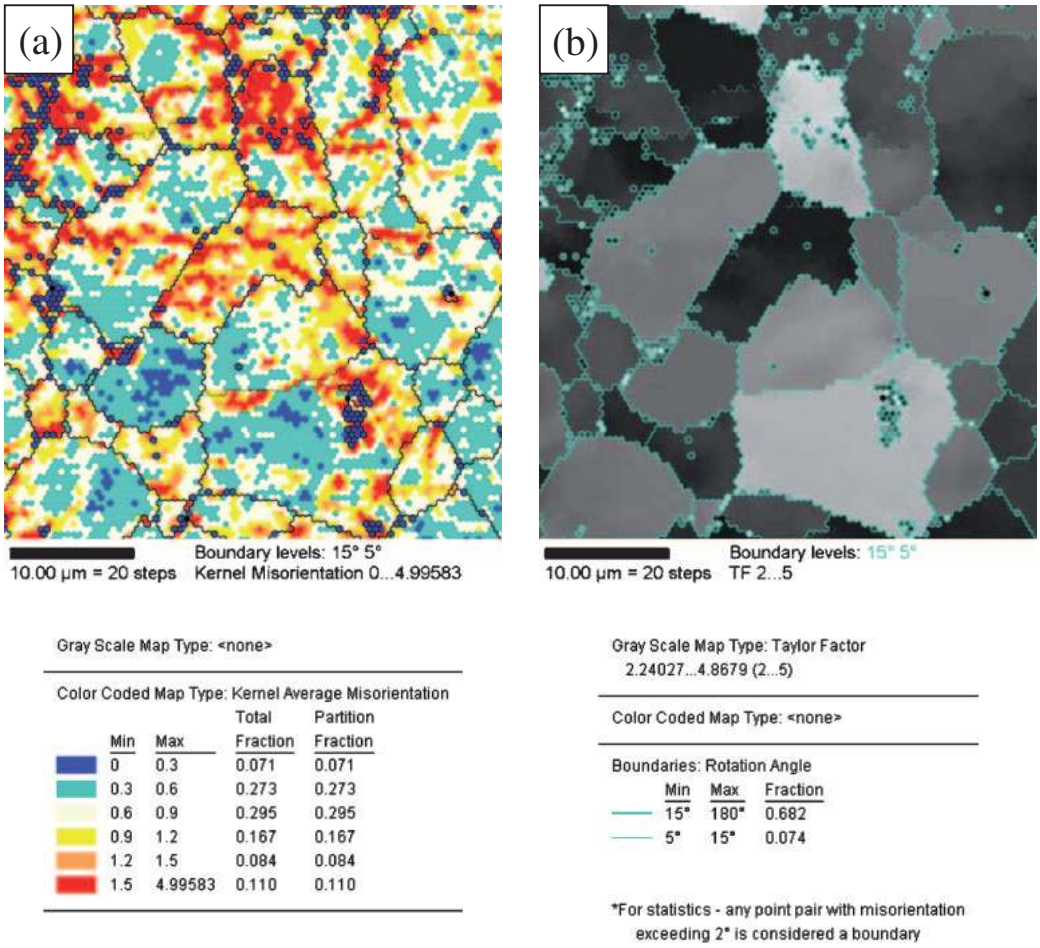

Fig. 7 Kernel average misorientation and Taylor factor maps in a LTF grain and HTF neighbors.

of the central grain is a small value of 2.52. In gray scale ('white' is high) used in Fig. 7(b), the TF of this grain is much lower than the TFs of the neighbors. The Taylor factor is essentially a measure of the influence of a grain's lattice orientation on its resistance to deformation. The LTF grain sometimes behaves as the soft one in the vicinity of the hard one. This case is, therefore, a typical example that macroscopic strain during deformation was accommodated by the "soft" and "hard" oriented grains.[1)] Further, the high strain area observed within the grain located above the central grain have the orientation P $\{011\}\langle 122\rangle$ which is one of recrystallization texture components obtained after annealing in cold rolled sheets of Al and Al alloys.[20)] The KAM and the TF for the P-orientated area within a tolerance of 10° are 1.50 and 4.51, respectively.

Another field including a high strain area is displayed in Fig. 8. The high strain part passes through area of several grains in Fig. 8(a). The grains in this area are classified using the Taylor factor into two groups. One is low TF, and another is higher. The KAM, the TF and the SF for the grains numbered in Fig. 8(b) are listed in Table 3. Very large strain is imposed on the low TF grains: No. 1, 5 and 7. On the other hand, the high TF grains having No. 3, 6, 9 and 10 have stored *relatively* small strain. For both the low and high TF grains, the SF is large enough that the slips initiate in them. Consequently, we conclude that in the high strain part passing through the grains, the initiation of slip occurs in a grain with high SF, and then the slip extends to neighbors. Then, the low TF grains sometimes deform in stead of the high TF grains, which should deform intrinsically with the larger total shear strain according to Taylor model with the underlying assumption. Thus, the deformation or strain is concentrated in not only the high TF but also some low TF grains.

6.2 Cube grains

Cube oriented subgrains are known to recover more rapidly than other orientations in rolled aluminum sheets, which results in a size advantage for the cube nuclei and, hence, a very good prospect for successful nucleation events.[20)] In a $\langle 001\rangle$ aluminum single crystal deformed in tension, the polygonal cell structure with loose dislocation walls were observed, in which no recrystallization occurred after annealing.[21)] This means that the microstructure without dense dislocation walls forms in the cube oriented grain deformed in tension of RD.

Here, in order to clarify the reason for the rapid recovery of the cube oriented subgrain, the stored energy or the KAM is examined for Cube grains. Figure 9 shows the KAM and Cube orientation maps for the object area. Comparison of the two maps reveals that the Cube grains do not store much energy during the CCB processing. The KAM values are

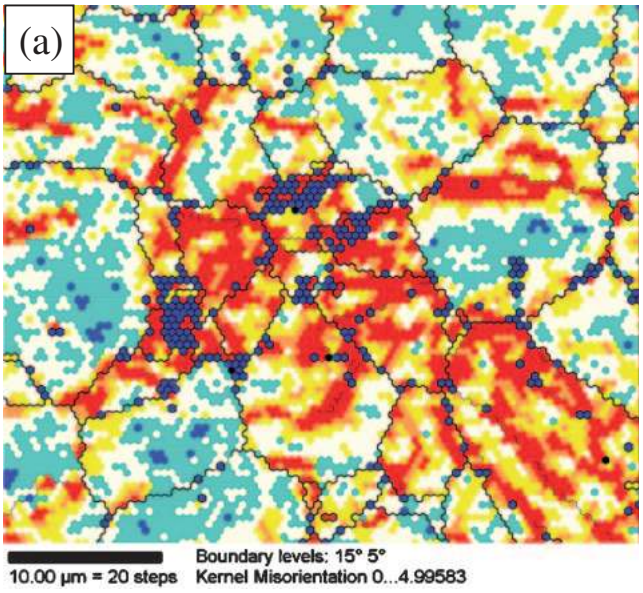

Color Coded Map Type: Kernel Average Misorientation

	Min	Max	Total Fraction	Partition Fraction
	0	0.3	0.051	0.051
	0.3	0.6	0.209	0.209
	0.6	0.9	0.299	0.299
	0.9	1.2	0.184	0.184
	1.2	1.5	0.090	0.090
	1.5	4.99583	0.166	0.166

Boundaries: Rotation Angle

Min	Max	Fraction
15°	180°	0.603
5°	15°	0.071

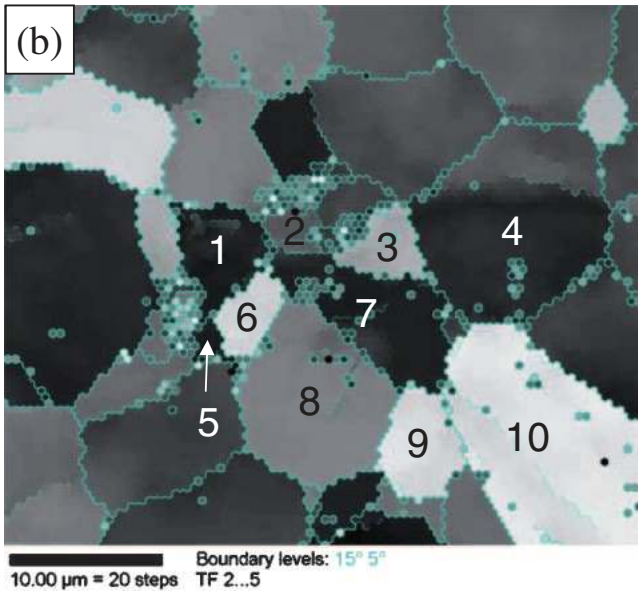

Gray Scale Map Type: Taylor Factor
2.1542...4.85041 (2...5)

Color Coded Map Type: <none>

Boundaries: Rotation Angle

Min	Max	Fraction
15°	180°	0.603
5°	15°	0.071

Fig. 8 Kernel average misorientation and Taylor factor maps for LTF grains and their neighbors.

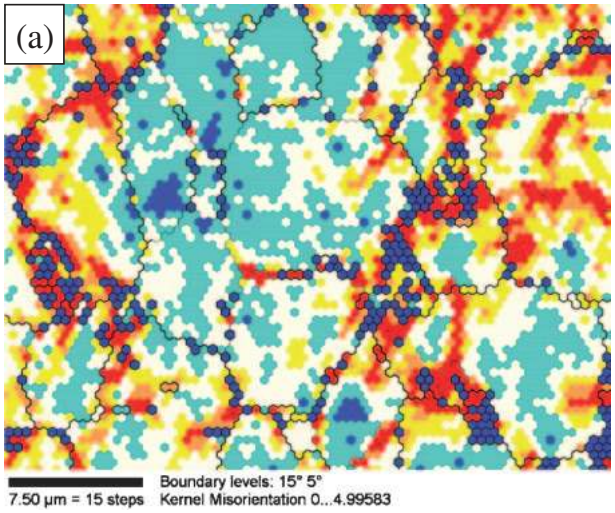

Gray Scale Map Type: <none>

Color Coded Map Type: Kernel Average Misorientation

	Min	Max	Total Fraction	Partition Fraction
	0	0.3	0.086	0.086
	0.3	0.6	0.260	0.260
	0.6	0.9	0.313	0.313
	0.9	1.2	0.164	0.164
	1.2	1.5	0.075	0.075
	1.5	4.99583	0.102	0.102

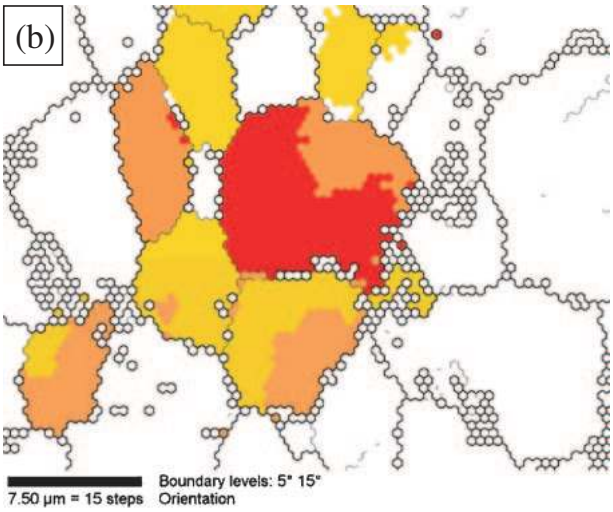

Gray Scale Map Type: <none>

Color Coded Map Type: Crystal Orientation

	Orientation Euler Angles	Orientation (hk(i)l)<uv(t)w>	Min	Max	Total Fraction	Partition Fraction
	(0.0, 0.0, 0.0)	(0 0 1)<1 0 0>	0°	5°	0.070	0.070
	(0.0, 0.0, 0.0)	(0 0 1)<1 0 0>	5°	10°	0.102	0.102
	(0.0, 0.0, 0.0)	(0 0 1)<1 0 0>	10°	15°	0.127	0.127

Fig. 9 Kernel average misorientation and Cube orientation maps for Cube grains and their neighbors.

Table 3 Kernel average misorientation and Taylor and Schmid factors for the grains in the high strain area. KAM: Kernel average misorientation, TF: Taylor factor, SF_RD and SF_TD: Schmid factors for uniaxial tension in rolling and transverse directions, respectively.

Grain No.	KAM/degree	TF	SF_RD	SF_TD	Note
1	1.813	2.45	0.465	0.458	ND 45° rotated Cube
2	1.624	3.16	0.483	0.467	
3	1.598	4.10	0.336	0.486	Near {011}⟨111⟩
4	0.963	2.71	0.439	0.443	Cube
5	1.952	2.39	0.445	0.441	Goss
6	1.514	4.56	0.429	0.465	P {011}⟨122⟩
7	1.501	2.47	0.441	0.495	Near RD rotated Cube
8	1.176	3.62	0.322	0.446	Cu
9	1.320	4.63	0.457	0.484	
10	1.447	4.71	0.449	0.466	P {011}⟨111⟩

measured as 0.641, 0.684 and 0.667 for the Cube oriented areas within tolerances of 5°, 10° and 15° from the ideal Cube orientation, respectively. These values are much smaller than a value of 0.980 obtained for the whole area measured (Fig. 4). This fact is consistent with the previous result obtained in the Al single crystal deformed in tension.[21] The slight difference in the three areas indicates that the deviation of 15° from the ideal orientation does not injure the predominance of the Cube oriented area. The small amount of the strain energy is one of the factors facilitating the rapid recovery of the Cube orientation. However, the vicinity of grain boundary is deformed even for the Cube grains. Such an area was found in the plural fields.

7. The Stored Energy Analysis Based on SEM/EBSP Data

7.1 Analysis by Image quality

Image quality parameter (IQ) describes the quality of an electron backscatter diffraction pattern. While the IQ is dependent on the material and its condition, it is not an absolute value but a function of the technique and the other processing parameters. However, the factor affecting the quality of diffraction patterns is the perfection of the crystal lattice in the diffracting volume. Thus, the IQ parameter can be used to give a quantitative description of the strain distribution in a microstructure. In a recent study, the image quality parameter was applied to analyze recrystallized volume fraction.[22] Figure 10 shows relation between the Image quality and the Taylor factor in the present sample. Although change in the Image quality is not so large but with a considerable scatter against the Taylor factor, it seems to correspond to change in the KAM (Fig. 6). The image quality may also be related to dislocation density because it is directly related to distortion in the crystal lattice.

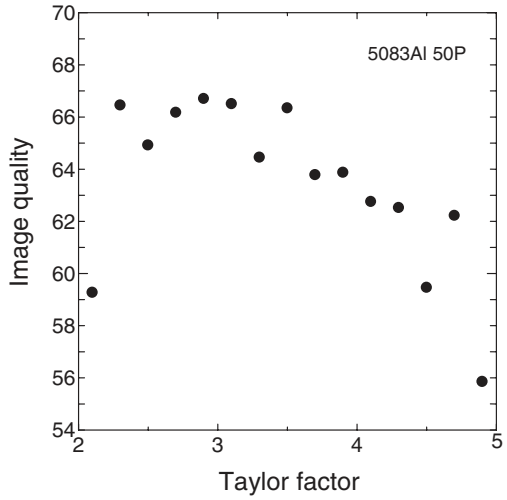

Fig. 10 Relation between image quality and Taylor factor in a 50-pass CCBent sample.

7.2 Calculation of stored energy from KAM

The KAM was calculated as an average value for misorientations within 5°, as mentioned above. Thus, the dislocation density can be derived from the calculation in an array of dislocations as well as a low angle boundary, though it should be underestimated because of existence of dislocations that do not contribute nor build up the misorientation. While a low angle tilt boundary consists of edge dislocations,[23] a low angle twist boundary screw dislocations.[24] If the spacing of the dislocations of Burgers vector $\boldsymbol{b}$ in the boundary is $\boldsymbol{h}$, then the crystals on either side for both types of the low angle boundaries are misoriented by a small angle θ [rad], where

$$\theta \approx 2\sin\frac{\theta}{2} = \frac{b}{h}. \tag{1}$$

This equation, which is simplified, is often called Frank's formula.[25,26] When the distance between points misoriented, namely 'step size' for the EBSP analysis is d, the area of boundary planes between the neighboring points per unit volume is represented by the peripheral length l and area a of a hexagon including a point, in consideration of unit thickness as

$$(l/a)/2 = \{2\sqrt{3}d/(\sqrt{3}d^2/2)\}/2 = 2/d.$$

Then, the length of dislocation lines per unit area of the boundary planes is α/h, where α is a constant which depends on the geometry of the dislocation arrangement. The values of α are 2 and 4 for pure tilt and twist boundaries, respectively. The dislocation density is given by the product

of the boundary plane area unit volume and the dislocation line length per unit area, as follows:[27)]

$$\rho \approx \frac{\alpha\theta}{bd}. \tag{2}$$

In the present study, d is fixed as 0.5 μm, b is 0.286 [nm] for aluminum and α is chosen to be 3 for boundaries of mixed character. The KAMs of the 50P and the as-received sample, 0P are 0.0171 [rad] (0.980 [degrees]) and 6.86×10^{-3} [rad] (0.393 [degrees]), respectively. Substituting the difference in the KAM for θ, the dislocation density, ρ [m^{-2}] is calculated as 2.15×10^{14} [m^{-2}]. The density should be underestimated as mentioned above. The stored energy per unit volume is obtained by the next equation.

$$E = \frac{1}{2}\alpha\rho Gb^2 \approx \frac{\alpha\theta Gb}{2d} \tag{3}$$

where G is the shear modulus and 26.1 [GPa] for an aluminum. Thus, $E = 2.3$ [J/mol]. This value is equivalent to the previous stored energy data of 30% cold-rolled aluminum,[27)] while it is smaller than the data of aluminum and its alloy obtained using the X-ray diffraction technique.[9)] The latter fact is probably due to the difference in volume of material investigated and different methods of measurements. In the same way, the KAM of each orientation gives $E = 6.1$ [J/mol] for a Goss grain (No. 5 in Table 3) and $E = 0.097$ [J/mol] for the Cube-oriented area within a tolerance of 5°. It is found in the CCBent sample that the stored energy for the Goss grain is more than 60 times higher than that for the Cube-oriented area.

8. Summary

The relation between the stored energy and the Taylor factor has been studied successfully in the Al-Mg-Mn alloy sheet worked by the continuous cyclic bending. The CCB had the decisive advantage of imposing no apparent rotation of grains during straining in spite of giving very large strain to sheet metals. First, the intragranular misorientations were examined to find the basic features of grains and their relation with the Taylor factor. Next, the relation between the kernel average misorientation (KAM) and the Taylor factor was investigated in details. It should be emphasized that whereas the KAM for the HTF region is large as expected, the KAM increases significantly with the decrease of the Taylor factor in the low TF range. Further analysis revealed Schmid factor effect on the energy stored during deformation. Then, the local strain analysis based on the KAM was carried out to find that macroscopic strain during deformation was accommodated by the "soft" oriented grain having the low TF. It was confirmed that the Cube oriented area has a low stored energy after the CCB. Finally, the relation between the stored energy and the image quality, which is one of the parameters obtained from the SEM/EBSP analysis, was discussed. Further, the dislocation density and the stored energy were derived from the calculation based on the KAM to compare the values in differently oriented grains.

Acknowledgements

One of the authors (Y. T.) gratefully acknowledges the financial support by the Light Metal Educational Foundation inc., Japan.

REFERENCES

1) W. B. Hutchinson: Int. Metals Rev. **29** (1984) 25–42.
2) B. L. Averbach, M. B. Bever, M. F. Comerford and J. S. Leach: Acta Metall. **4** (1956) 477–484.
3) H. U. Astron: Acta Metall. **3** (1955) 508–509.
4) M. Matsuo, S. Hayami and S. Nagashima: Adv. X-ray Anal. **14** (1971) 214–230.
5) H. Takechi, H. Katoh and S. Nagashima: Trans. AIME **242** (1968) 56–65.
6) R. L. Every and M. Hartherly: Texture **1** (1974) 183–194.
7) J. S. Kalland and Y. C. Huang: Metal Sci. **18** (1984) 381–385.
8) N. Rajmohan, Y. Hayakawa, J. A. Szpunar and J. H. Root: Acta Mater. **45** (1997) 2485–2494.
9) N. Rajmohan and J. A. Szpunar: Mater. Sci. Tech. **15** (1999) 1259–1265.
10) Ph. Gerber, J. Tarasiuk, Th. Chauveau and B. Bacroix: Acta Mater. **51** (2003) 6359–6371.
11) G. I. Taylor: J. Inst. Met. **62** (1938) 307–324.
12) B. L. Adams, S. I. Wright and K. Kunze: Metall. Trans. **24A** (1993) 819–831.
13) S. I. Wright, D. P. Field and D. J. Dingley: *Electron Backscatter Diffraction in Materials Science*, Eds. A. J. Schwartz, M. Kumar and B. L. Adams, (Kluwer Academic, 2000) chp. 13.
14) Y. Takayama, M. Yamaguchi, T. Tozawa, H. Kato, H. Watanabe and T. Izawa: *Proc. fourth Intern. Conf. on Recrystallization and Related Phenomena (JIMIS10)*, (The Japan Institute of Metals, 1999) pp. 321–326.
15) Y. Takayama, J. A. Szpunar and H. T. Jeong: Mater. Trans. **42** (2001) 2050–2058.
16) Y. Takayama, Y. Saigo, R. Takahashi and H. Kato: J. Japan Inst. Light Metals **52** (2002) 566–571.
17) G. S. Sangdahl, Jr, E. L. Aul and G. Sachs: Proc. Soc. Exp. Stress Analysis **6** (1948) 1–18.
18) B. Bacroix, Ph. Gerber and O. Castelnau: *Proc. First Joint Intern. Conf. Recrystallization and Grain Growth*, Eds. G. Gottstein and D. A. Molodov, (Springer-Verlag, 2001) p. 623–633.
19) E. Sachs: Z. Ver. dt. Ing. **72** (1928) 734 [quoted from J. Hirsh and K. Lücke, Acta Metall., **36** (1988) 2883–2904. Ref. 4].
20) O. Engler: Mater. Sci. Tech. **12** (1996) 859–872.
21) M. Tagami, K. Kashihara, T. Okada and F. Inoko: J. Japan Inst. Metals **64** (2000) 535–542.
22) J. Tarasiuk, Ph. Gerber and B. Bacroix: Acta Mater. **50** (2002) 1467–1477.
23) J. F. Humphreys and M. Hatherley: *Recrystallization and Related Annealing Phenomena*, (Elsevier Science, 1995) pp. 60–63.
24) S. E. Babcock and R. W. Balluffii: Philos. Mag. **A55** (1987) 643–653.
25) F. C. Frank: *Report on the Symposium on the Plastic Deformation of Crystalline Solids*, (Carnegie Institute of Technology, Pittsburgh, 1950) pp. 150–154.
26) D. A. Hughes, S. M. A. Khan, A. Godfrey and H. M. Zbib: Mater. Sci. Engg. **A309–310** (2001) 220–226.
27) Q. Liu, D. J. Jensen and N. Hansen: Acta Mater. **46** (1998) 5819–5838.